IEEE Access
Multidisciplinary | Rapid Review | Open Access Journal

Received August 14, 2020, accepted September 2, 2020, date of publication September 8, 2020,
date of current version September 22, 2020.

Digital Object Identifier 10.1109/ACCESS.2020.3022790

A Multiobjective Optimization Approach for Extended Interaction Oscillators

JIAN CUI, SHURONG BIAN, AND AIDI LI
Information School, North China University of Technology, Beijing 100144, China

Corresponding author: Jian Cui (cuijian513420@163.com)

This work was supported by the Fundamental Research Business Expenses Program of Universities Affiliated to Beijing under Grant 110052971921/006.

ABSTRACT The development of high-frequency, wide-bandwidth, high-power extended interaction oscillators (EIOs) has always been the focus of researchers working on millimeter-wave and terahertz electronic devices. However, these design objectives are affected by many structural and operating parameters, and traditional manual optimization and local optimization are no longer suitable for solving these problems. In this paper, based on a one-dimensional, nonlinear, self-consistent program of EIOs, a multiobjective optimization method that employs the nondominated sorting genetic algorithm II (NSGA-II) is proposed to simultaneously optimize device output power, bandwidth, and structure length. By using this approach, the optimization process of a 95-GHz EIO is presented, and the corresponding Pareto solutions are obtained after 500 generations with a population size of 50. The results show that the beam-wave interaction and the coupling mechanism lead to synchronization of the structural parameters and the electrical parameters with each other, and the coexistence of multiple objectives guides the zonal distribution of the optimal solutions. That is, the oscillators with fewer gaps have shorter structure length and higher power, whereas those with more gaps are prone to start oscillation and have wider bandwidth. Several sets of optimization results obtained using the proposed method agree well with the results obtained in the CST-PIC solver, which proves that the proposed algorithm is effective for optimizing EIOs because it considers multiple design goals and can serve as a theoretical basis for engineering development.

INDEX TERMS Extended interaction oscillators, nonlinear self-consistent theory, nondominated sorting genetic algorithm II, multiobjective optimization.

I. INTRODUCTION

An extended interaction oscillator (EIO) is a kind of vacuum electronic device that combines the advantages of klystron and traveling wave tube to offer high power, high efficiency, and wide bandwidth [1], [2]. It has emerged as an important high-power source device for use in the millimeter-wave to terahertz band [3], [4] and has been widely used in satellite communication, climate observation, deep space topology imaging, and other radar systems [5]–[8].

As shown in Fig. 1 [6], the interaction structure of an EIO is usually composed of a slow-wave structure that is short-circuited at both ends. The beam-wave interaction may occur in multiple gaps, which can increase the interaction length and increase the effectiveness of the energy exchange between electron beams and electromagnetic waves [9].

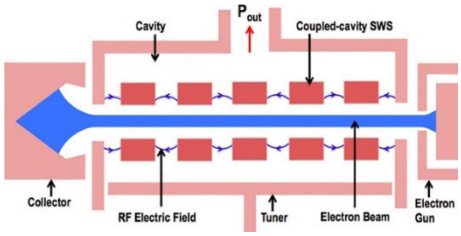

FIGURE 1. Block diagram of EIO.

As the number of gaps increases, the enlarged internal surface area can disperse the energy of the resonant cavity, improve heat dissipation in the tube, reduce the possibility of breakdown, and effectively enhance the power capacity of the device in the millimeter/terahertz wavelength band. However, there remain many limitations in this direction. Theoretically, more gaps can lead to higher output power and

The associate editor coordinating the review of this manuscript and approving it for publication was Hisao Ishibuchi.

conversion efficiency, but they may also cause electron overclustering, thus reducing output efficiency. By contrast, fewer gaps may cause problems such as reduction in the quality factor, lack of self-oscillation inside the resonator, and narrow output bandwidth. Therefore, in the case of EIO devices, a large number of structural and working parameters need to be deigned and optimized.

Recently, many studies on the optimization of EIOs have been conducted. Zhiwei Chang *et al.* introduced an extended interaction klystron with a working voltage of 5 kV based on the traditional power bandwidth factor $M^2(R/Q)$ [10]. Hooman Bahman Soltani *et al.* optimized a 12-gap EIO from the viewpoint of output power and electronic tuning bandwidth based on the ''electron beam line'' of beam–wave interaction and the ''load line'' of coupling output power [11]. Shuyuan Chen *et al.* analyzed the influence of the coupling loss and external quality factor on the output power of extended interaction klystrons and designed a five-gap output structure for extended interaction klystrons [12]. These examples of traditional design and optimization can clearly describe the influence of each parameter on output power or starting state and can improve device performance to a certain extent. However, the one-dimensional (1D) parameter scanning method can only be used for local optimization, and it is difficult to achieve global optimization of many structural and working parameters.

Xuxun Ren *et al.* optimized the length and gap width of the last three cycles of an oscillator by using a genetic algorithm and realized a significant increase in the device output power [13]. Based on deterministic sampling methods, Hien Tran *et al.* selected the position and frequency of the cavity, which greatly influence the output characteristics, as the input parameters, realized automatic design optimization of klystrons, and significantly improved the optimization efficiency [14]. From the many parameters of klystrons, they selected a few key parameters to realize multi-dimensional optimization of local parameters, so the initial values of these parameters were crucial. Zaigao Chen *et al.* performed high-power global optimization of a backward wave tube Bragg reflector by adjusting its geometric structure parameters and working parameters by using a parallel genetic algorithm [15]. However, this optimization was limited to only objective of output power or efficiency, without consideration of the co-transition of multiple objectives.

Christopher James Lingwood *et al.* used a multiobjective genetic algorithm to globally optimize a klystron, with a focus on efficiency and tube length. The effectiveness of the algorithm was verified by comparing the optimized parameters with those of the B-factor klystron developed by Stanford Linear Accelerator Center [16]. However, only two objectives were optimized, whereas oscillators may have multiple design objectives that constrain each other. This problem of coexisting objectives has always been the focus of researchers working on EIOs.

In this paper, a 1D simulation program that can be used to calculate the output characteristics of EIOs is proposed. Then, by using the proposed simulation program, an automatic optimization routine is developed by using the nondominated sorting genetic algorithm II (NSGA-II) [17], which has been proved to be an effective multiobjective search technique in various applications [18]–[21]. This method helps to enhance the performance of EIOs by considering multiple design objectives simultaneously. Finally, the proposed technique is applied to a W-band EIO, and the structural dimensions of the device and its operating conditions are considered free parameters. The optimization results and the corresponding parameters are evaluated and compared with those obtained using the CST-PIC solver [22].

II. METHODOLOGY

Genetic algorithms, which are global optimization algorithms, adopt the random search method. In contrast to traditional algorithms, genetic algorithms do not depend on gradient information. When the gradient method is applied to a large-scale problem, the problem complexity in space and time increases continuously. Genetic algorithms are widely used for high-dimensional large-scale optimization and to solve complex, multiobjective problems. The general steps of a genetic algorithm are as follows [23]–[25].

1. Define the search space. Genetic algorithms use the concept of ''individual'' to express the search space, which means that the search space can be expressed as given in (1) (2) [17]:

$$\{x, z, f, \gamma\} \in X \tag{1}$$

$$\{X_{(1)}, X_{(2)}, X_{(3)}, \ldots, X_{(P)}\} \in P \tag{2}$$

where x represents the decision vector, z the solution vector, f the fitness of x, γ the ranking score, and P the population quantity; X is called an individual.

2. Select the individual. This step focuses more on the search space with higher average fitness to improve the average quality of the population [26].

3. Cross and mutate between selected individuals. This step involves generating new individuals and enhancing the search ability of the algorithm.

In NSGA-II, Pareto sets are used to obtain the optimal solution for more than one objective. Thus, EIO design can be described as a multiobjective global optimization problem, and when compared with NSGA-II, the decision vector x is an EIO structure with multiple parameters $x = [x^1, x^2, \ldots, x^n]$, and the solution vector z is the design objective $z = [z^1, z^2, \ldots, z^n]$. Moreover, fitness f and ranking score γ can be obtained using the proposed 1D EIO simulation program. However, NSGA-II cannot identify EIO structures that have no physical meaning, and if there are many bad solutions, the effectiveness and convergence of the algorithm may deteriorate considerably. Therefore, the choices of the decision vector, solution vector, and parameter ranges for each dimension of the decision vector are important.

A. 1D EIO MODEL

In the EIO high-frequency interaction structure, an electron beam excites electromagnetic waves during the movement, and the electromagnetic waves react to the electron beam. Thus, these two processes affect each other and generate energy exchange [27]. Based on 1D electronic disk model and the power balance theory, the optimization process can be described as follows:

1) HIGH-FREQUENCY FIELD

Considering that the beam–wave interaction mainly occurs at the gap center in the cavity, the high-frequency electric field along the z- axis direction can be expressed equivalently by the following functional equation:

$$E_Z = f(t)f(z)\sin(\omega t + \phi_0) \tag{3}$$

$$f(z) = \sum_{n=1}^{N} V_n \frac{k}{\sqrt{\pi}} e^{-k^2(z-z_0)^2} \tag{4}$$

where $f(t)$ is the voltage across gaps in the resonator, $f(z)$ the electronic field type of Gaussian distribution [28], $k = 1/\sqrt{r_a^2 - r_b^2 + \delta d^2}$, z_0 the center position of each gap, r_a the drift tube radius, r_b the electron beam radius, and d the gap width; δ reflects the influence of the drift head shape on the field type, and it is generally taken as 1/6–1/2. N denotes the number of gaps, and V_n is the normalized relative amplitude of each gap voltage without considering the influence of the output waveguide on the electric field distribution, $V_1 = V_2 = \ldots = V_n$.

2) KINEMATIC EQUATION OF ELECTRON BEAM

Because the velocity of electrons is considerably lower than the velocity of light, the relativistic effect is neglected, and considering the interaction of space charge forces among electrons, the equation of motion in the high-frequency interaction structure can be written as follows:

$$dv/dt = -\eta(E_z + E_s) \tag{5}$$

where η is the charge-to-mass ratio, and E_s is the space charge force among electrons. For a cylindrical electron beam, the approximate expression of the space charge electric field E_s can be obtained as follows [28]:

$$E_s(z) = \int \frac{\tau(z')}{2\pi\varepsilon_0 b^2} e^{-\frac{2|z'-z|}{b}} sign(z'-z)\, dz' \tag{6}$$

where τ denotes the linear charge density of the electron beam at z, ε_0 represents the vacuum dielectric constant, and sign(x) is a symbolic function.

3) SELF-CONSISTENT EQUATION

The power balance between the output energy coupled out through the waveguide and the energy released by the electron beam (regardless of cavity loss) can be described as follows [29]–[31]:

$$dW(t) = -P_{out}dt + P_b dt \tag{7}$$

where $W(t)$ is the stored energy, P_{out} the output power of the EIO, P_b the exchanged energy, and their respective expressions are as follows:

$$P_{out} = \frac{1}{2} \cdot \frac{f(t)^2}{Q_e} \cdot (R/Q) \tag{8}$$

$$P_b = \int_L \tau \cdot E_z dl \tag{9}$$

where (R/Q) represents the impedance of the cavities [2], and it be expressed as

$$(R/Q) = \left(\int_L |E_Z|dl\right)^2 \Big/ 2\omega W(t). \tag{10}$$

By substituting (7), (8), and (9) into (6), the voltage variation equation of the microwave field in the resonator can be obtained as

$$\frac{df(t)}{dt} = -\frac{\omega f(t)}{2Q_e} + \omega \cdot (R/Q) \int \tau v f(z) \sin(\omega t + \varphi_0) dz. \tag{11}$$

4) 1D SIMULATION PROGRAM

Based on the 1D electron disk beam–wave interaction calculation model, the continuous electron beam is replaced with a finite electron disk, and (5) and (11) can be rewritten as follows:

$$\frac{dv_i}{dt} = -\eta\left(E_z(z,i) + E_s(z,i)\right) \tag{12}$$

$$\frac{df(t)}{dt} = -\frac{\omega f(t)}{2Q_e} + \omega(R/Q)\sum_{i=1}^{i=M} q_i v_i \cdot f(z,i)\sin(\omega t + \phi_0) \tag{13}$$

where q_i is the amount of electricity carried by the i-th disk.

These differential equations can be solved by means of programing using the fourth-order Runge–Kutta method. A flowchart of the program is shown in Fig. 2.

1. Initialize various EIO parameters, including operating parameters, structural parameters, cold measurement parameters, such as beam voltage V_0, current I_0, gap width d, period length l, characteristic impedance (R/Q), and quality factor Q_e.
2. Place electronic disks equidistantly with respect to the resonator entrance and inject them with a certain initial velocity. By using the fourth-order Runge–Kutta method, the position and velocity of the electronic disks are solved after a time step under the current electric field.
3. According to the position and speed of each disk, the energy exchange between the disk and the electric field is calculated to obtain a new electric field amplitude, and this value is compared with the previous electric field amplitude to check for convergence.
4. If the result does not fulfill the convergence condition, add new disks at the initial position and repeat 2; else, calculate the output power, bandwidth, and structure length.

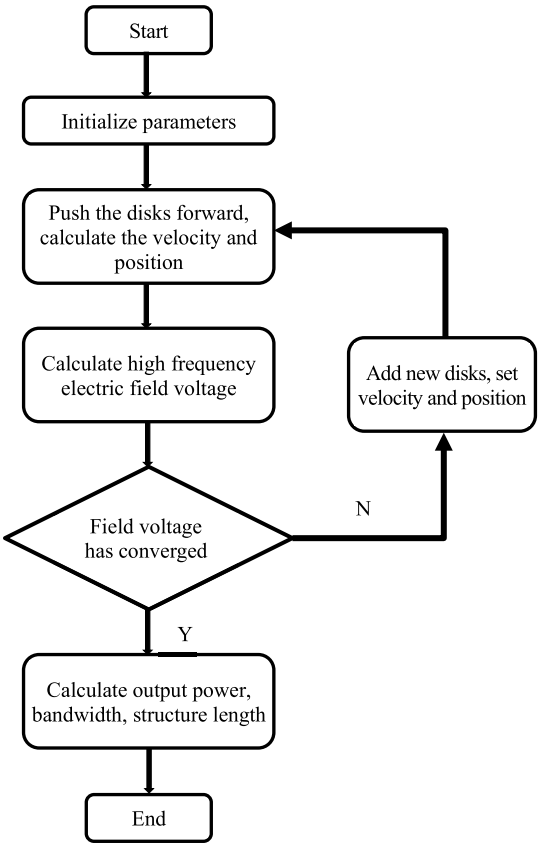

FIGURE 2. The flow chart of the EIO 1D program.

B. OPTIMIZATION ALGORITHM

In EIO design, the key is obtaining a high-frequency interaction structure with high power capacity, wide bandwidth, and stable single-mode operation. Due to the limited number of gaps in EIOs, the corresponding synchronous voltage changes greatly compared with that of the ideal periodic structure. Moreover, the resonator has a high gap voltage in the gap, which induces a significant change in the electron velocity. Consequently, some electrons may exhibit the transcendence phenomenon, which is essentially a nonlinear physical phenomenon. In the process of motion, electrons are affected by the high-frequency field and the space charge field, and the electron density and electron velocity become multivalued functions. Therefore, analysis of the influences of electron velocity, distance between gaps (period length), number of gaps, space charge force, drift tube distance between resonators, and magnetic field strength on the beam–wave synchronization and coupling mechanism involves many complex calculations. Moreover, it is a tedious and time-consuming task to manually optimize the structure parameters and operating parameters to find a feasible configuration.

Numerous parameters have different effects on the output characteristics of EIOs. Moreover, because the design optimization of EIOs is a high-dimensional problem in both the decision space and the solution space, NSGA-II may be suitable for solving the high-dimensional optimization problem in conjunction with the proposed 1D simulation program. Based on previous EIO design experience, the decision vector and solution vector are defined in TABLE 1.

TABLE 1. Decision vector and solution vector.

Vector	Elements
Decision Vector	$[d, l, Q_e, r_b, V_0, I_0, N]$
Solution Vector	$[B, P_{out}, L_{tot,}]$

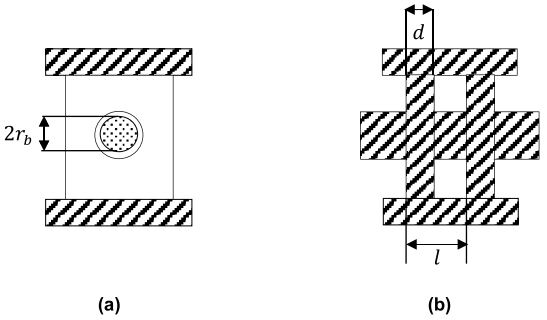

FIGURE 3. Schematic diagram of EIO (e.g., N = 2): (a) cross section and (b) longitudinal section.

For the decision vector, as shown in Fig. 3, d is the width of the cavity gap; l the EIO structure period; Q_e the external quality factor; r_b the radius of the beam in the drift tube; V_0 and I_0 the beam voltage and current, respectively; and N the cavity number.

For the solution vector, the output power P_{out} is selected as objective 1, which can be calculated using the 1D program (14). The bandwidth B is selected as objective 2 and defined as (15). The length of the interaction structure L_{tot} is selected as objective 3 and described as (16).

$$P_{out} = 1D(d, l, Q_e, r_b, V_0, I_0, N) \tag{14}$$

$$B = f_0 / Q_e \tag{15}$$

$$L_{tot} = N \cdot l \tag{16}$$

For EIOs, it is expected that higher output power and wider bandwidth can be obtained in shorter beam-wave interaction structures. However, in this process, the electron reversal phenomenon, which causes a sharp decrease in output power, must be avoided. Finally, the multiobjective optimization model of EIOs can be expressed as (17):

$$\begin{aligned} &\max : F_1 = P_{out}(d, l, Q_e, r_b, V_0, I_0, N) \\ &\max : F_2 = B(f, Q_e) \\ &\min : F_3 = L_{tot}(l, N) \\ &s.t.\ \min(v) > 0 \end{aligned} \tag{17}$$

A flowchart of the optimization algorithm is shown in Fig. 4.

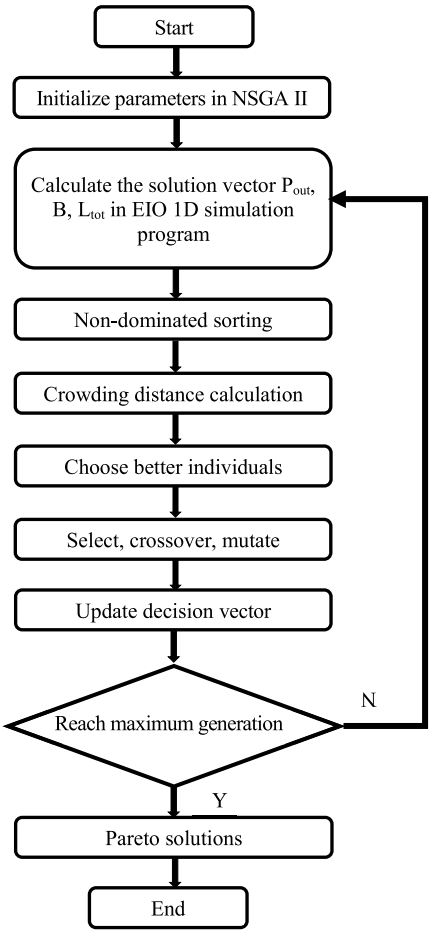

FIGURE 4. Flowchart of optimization algorithm.

1. Set the initial range of each parameter to determine the scope of the search space.
2. Calculate the EIO output characteristics (output power, structure length, and instantaneous bandwidth) by using the proposed 1D simulation program.
3. Sort the population based on nondomination, and assign crowding distance.
4. Select individuals with high scores to update the decision vector until the termination condition is reached.
5. Obtain a nondominant set containing individuals that fulfill the design specifications better.

III. RESULT AND ANALYSIS

In this section, a 95-GHz EIO is considered as a test problem for achieving higher output power, wider bandwidth, and shorter length. The scope of the search space plays a very important role in the EIO design process. For example, the beam voltage V_0 and current I_0 are directly related to the output power of the entire oscillator. The current I_0 may affect the oscillator startup time and the electron conversion efficiency. The beam voltage V_0 and the period length l are the basic synchronization conditions for the beam-wave of electrons and electromagnetic waves. In addition, the gap width d governs the interaction between the electrons and the electromagnetic waves in each cavity, which not only affects the beam–wave coupling coefficient but is also related to the characteristic impedance of the cavity. The external quality factor Q_e reflects the coupling output energy of the waveguide. The electron beam radius reflects the cross-sectional area when electrons interact with the electric field, and it generally does not exceed 80% of the drift tube radius. Considering of these factors, we set the range of decision vector as given in TABLE 2.

TABLE 2. Optimization scop of search space.

Parameter	Range
d (mm)	0.1-0.3
l (mm)	0.2-0.9
Q_e	200-2000
r_b (mm)	0.15-0.2
V_0 (kV)	9-19
I_0 (A)	0.1-0.5
N	5-9

Experiments were carried out with a population of 50 individuals, and the genetic algorithms were run for 500 iterations with a mutation probability of 1/7 and a crossover probability of 1. Fig. 5 shows that as the number of iterations increase, the output power and bandwidth are significantly concentrated in the upper right corner of the figure, which indicates that the optimization is moving toward higher power and wider bandwidth. After 300 iterations, the output power converges to 1400—2400 W, bandwidth converges to 74—475 MHz, and it is simple with zonal distribution.

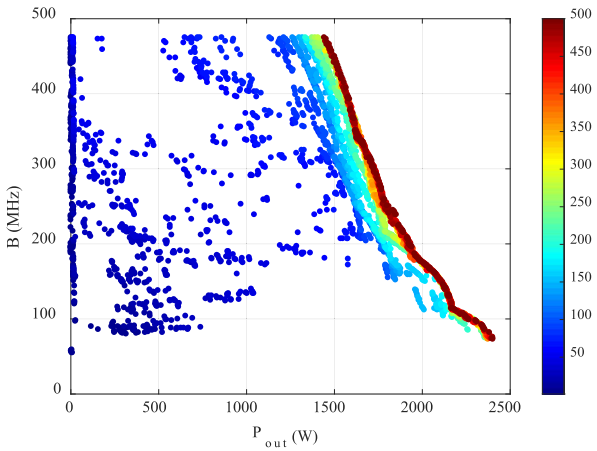

FIGURE 5. Evolution of the output power and bandwidth in the optimization process; the color map represents the number of iterations.

The instantaneous bandwidth was negatively correlated to the output power, indicating that the output power of the EIO was not the highest at the widest bandwidth. Notably, after a certain degree of bandwidth optimization, it was difficult to increase the bandwidth, and any further attempts may have led to a significant drop in the output power and conversion

efficiency or even failure of the EIO to start up. This can possibly be ascribed to fact that the lower external quality factor caused a greater amount of energy to be coupled out of the resonator through the waveguide, which was not conducive for establishing a sufficiently large electric field, thereby reducing the strength of the beam–wave interaction.

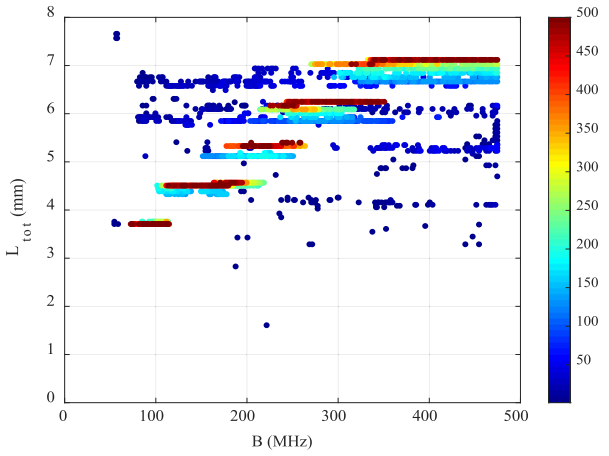

FIGURE 6. Evolution of the bandwidth and structure length in the optimization process; the color map represents the number of iterations.

Fig. 6 shows that the length of the interaction structure exhibits a clear differentiation trend during the optimization process, and it is distributed in a band shape around 3.7 mm, 4.5 mm, 5.3 mm, 6.2 mm, and 7.1 mm, and the corresponding gap number N is 5–9 in sequence. This means that to obtain a wider bandwidth, a longer interaction length is required. Moreover, it may be possible that the greater the number of gaps, the higher is the characteristic impedance of the resonant cavity, and it is prone to establish a stronger electric field, which can appropriately reduce the external quality factor and yield a wide bandwidth.

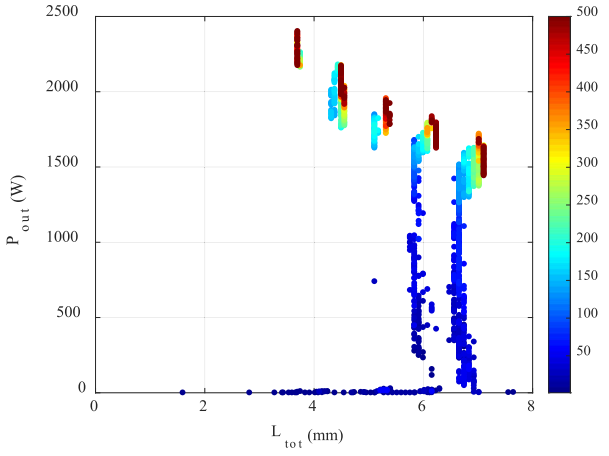

FIGURE 7. Evolution of the structure length and output power in the optimization process; the color map represents the number of iterations.

Fig. 7 shows that the length of the interaction structure in the initial stage is mainly concentrated around 6.2 mm and 7.1 mm, i.e., 8-gap and 9-gap EIO. As the number of iterations increases, the optimization begins to gradually expand toward high-power and short structures. Possibly, self-oscillations in the long structure are prone to build up during the initial optimization processes.

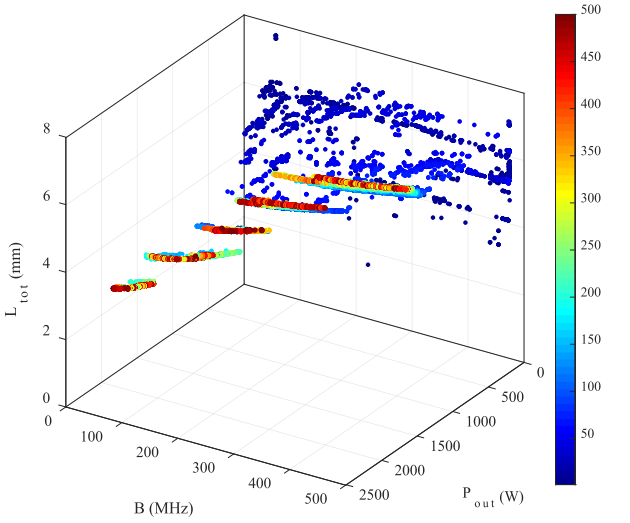

FIGURE 8. Evolution of the bandwidth, output power, and structure length in the optimization process; the color map represents the number of iterations.

Fig. 8 shows the optimization process involving the bandwidth, output power, and length of the interaction structure. As the number of iterations increases, these individuals are optimized toward wider bandwidth, higher power, and shorter length, and after 300 iterations, the individuals gradually tend exhibit a regular zonal distribution.

Based on the optimization solution vector, the final results were divided into five groups. As summarized in TABLE 3, the output power range of the 5-gap EIO is 2174—2401 W, and the shortest length of the interaction structure is 3.70 mm, whereas the corresponding bandwidth is generally narrow in 74—114 MHz region. As the number of gaps increases, the output power of the solutions in each group decreases, whereas the length and bandwidth increase significantly. The bandwidth of the 9-gap EIO is generally wide, ranging from 349 MHz to 475 MHz, whereas the length reaches 7.11 mm.

Based on the optimization decision vector, the gap width d is mainly concentrated in the 0.28–0.30 mm range. A shorter gap width is favorable for increasing the efficiency of beam–wave interaction, whereas a lower electric field strength and, correspondingly, characteristic impedance, reduce the total energy exchange. In this case, the electric field strength and the field pattern distribution are more conducive to electron bunching and energy exchange.

The period length l gradually increases with the number of gaps. This is because in the slow-wave interaction structure, only when the phase velocity of the electromagnetic field is slightly lower than the electron velocity, a significant beam–wave interaction occurs; subsequently, the electron beam releases energy into the electromagnetic field, and the

TABLE 3. The optimal solutions for the EIO.

NO.	Decision Vector							Solution Vector		
	d(mm)	l(mm)	Q_e	N	r_b(mm)	V_0(kV)	I_0(A)	B(MHz)	P_{out}(W)	L_{tot}(mm)
1	0.24	0.74	1281	5	0.20	19.00	0.50	74	2401	3.70
2	0.25	0.74	1158	5	0.20	19.00	0.50	82	2382	3.70
3	0.28	0.73	1108	5	0.20	19.00	0.50	86	2356	3.70
4	0.28	0.74	1032	5	0.20	19.00	0.50	92	2339	3.70
5	0.29	0.74	990	5	0.20	18.96	0.50	96	2312	3.70
6	0.29	0.74	975	5	0.20	18.96	0.50	97	2307	3.70
7	0.30	0.74	962	5	0.20	18.85	0.50	99	2266	3.70
8	0.30	0.74	905	5	0.20	18.85	0.50	105	2242	3.70
9	0.30	0.74	845	5	0.20	18.76	0.50	112	2187	3.70
10	0.30	0.73	837	5	0.20	18.75	0.50	114	2174	3.70
11	0.29	0.76	730	6	0.20	18.99	0.50	130	2156	4.50
12	0.29	0.75	660	6	0.20	18.98	0.50	144	2125	4.50
13	0.29	0.75	649	6	0.20	18.99	0.50	146	2119	4.50
14	0.29	0.75	589	6	0.20	19.00	0.50	161	2074	4.50
15	0.29	0.74	589	6	0.20	19.00	0.50	161	2074	4.50
16	0.29	0.75	566	6	0.20	19.00	0.50	168	2045	4.50
17	0.29	0.76	557	6	0.20	19.00	0.50	171	2023	4.56
18	0.29	0.75	538	6	0.20	18.98	0.50	177	1992	4.50
19	0.28	0.76	483	7	0.20	18.77	0.50	197	1933	5.32
20	0.28	0.76	483	7	0.20	18.77	0.50	197	1933	5.32
21	0.28	0.77	463	7	0.20	18.99	0.50	205	1922	5.39
22	0.28	0.76	455	7	0.20	18.84	0.50	209	1915	5.32
23	0.28	0.76	441	7	0.20	18.78	0.50	215	1894	5.32
24	0.27	0.76	423	7	0.20	18.74	0.50	225	1868	5.32
25	0.28	0.78	398	7	0.20	18.99	0.50	239	1852	5.39
26	0.28	0.78	387	7	0.20	18.99	0.50	245	1833	5.39
28	0.28	0.78	367	7	0.20	18.99	0.50	259	1786	5.39
27	0.28	0.78	379	8	0.20	18.99	0.50	251	1799	6.16
29	0.29	0.78	346	8	0.20	19.00	0.50	275	1768	6.24
30	0.29	0.78	342	8	0.20	19.00	0.50	278	1758	6.24
31	0.29	0.78	332	8	0.20	18.99	0.50	286	1746	6.24
32	0.29	0.78	315	8	0.20	18.98	0.50	302	1724	6.24
33	0.29	0.79	314	8	0.20	18.98	0.50	303	1714	6.24
34	0.29	0.78	302	8	0.20	18.99	0.50	315	1698	6.24
35	0.29	0.78	287	8	0.20	18.98	0.50	331	1667	6.24
36	0.28	0.78	282	8	0.20	18.99	0.50	337	1658	6.24
37	0.29	0.78	277	8	0.20	18.98	0.50	343	1641	6.24
38	0.29	0.79	272	9	0.20	18.99	0.50	349	1627	7.11
39	0.29	0.79	271	9	0.20	18.99	0.50	351	1617	7.11
40	0.29	0.79	259	9	0.20	19.00	0.50	367	1612	7.11
41	0.29	0.79	258	9	0.20	19.00	0.50	368	1602	7.11
42	0.29	0.79	250	9	0.20	18.99	0.50	380	1594	7.11
43	0.29	0.79	242	9	0.20	19.00	0.50	393	1586	7.11
44	0.29	0.79	233	9	0.20	19.00	0.50	408	1567	7.11
45	0.29	0.79	225	9	0.20	18.99	0.50	422	1543	7.11
46	0.29	0.79	219	9	0.20	18.98	0.50	434	1525	7.11
47	0.29	0.80	211	9	0.20	18.99	0.50	450	1501	7.11
48	0.29	0.80	208	9	0.20	18.99	0.50	457	1484	7.11
49	0.29	0.78	200	9	0.20	18.97	0.50	475	1442	7.11
50	0.29	0.79	200	9	0.20	18.99	0.50	475	1442	7.11

oscillator is prone to oscillate. The period length is related to the phase velocity of electromagnetic field, and the beam voltage is related to the electron velocity. According to the beam–wave synchronous coupling principle, each voltage has its corresponding period length [32], and as the number of gaps increase, the length of the corresponding synchronization period gradually increases.

The number of gaps N and the external quality factor Q_e show a negative correlation, probably because of low characteristic impedance with fewer gaps; the short beam-wave interaction length makes it difficult for the oscillator to start up; and increasing external quality factor can cause the resonator to build up a strong enough electric field at the start of the oscillation, improve the beam-wave interaction and cause the electron beam to release more energy. On the other hand, the electron beam may form an excessive cluster with more gaps, which would weaken the bunching effect and reduce the output power. However, due to the high characteristic impedance, the oscillations can build up at a low external quality factor, which would help obtain a wide instantaneous bandwidth. Therefore, the optimization results of the external quality factor and number of gaps not only reflect the high-power requirements of the oscillator but also consider the broadband target and the structure length.

The electron beam radius quickly converged to 0.2 mm, which means that the electron beam radius was positively related to the design objective. This is due to the weak equivalent space charge force with the large electron

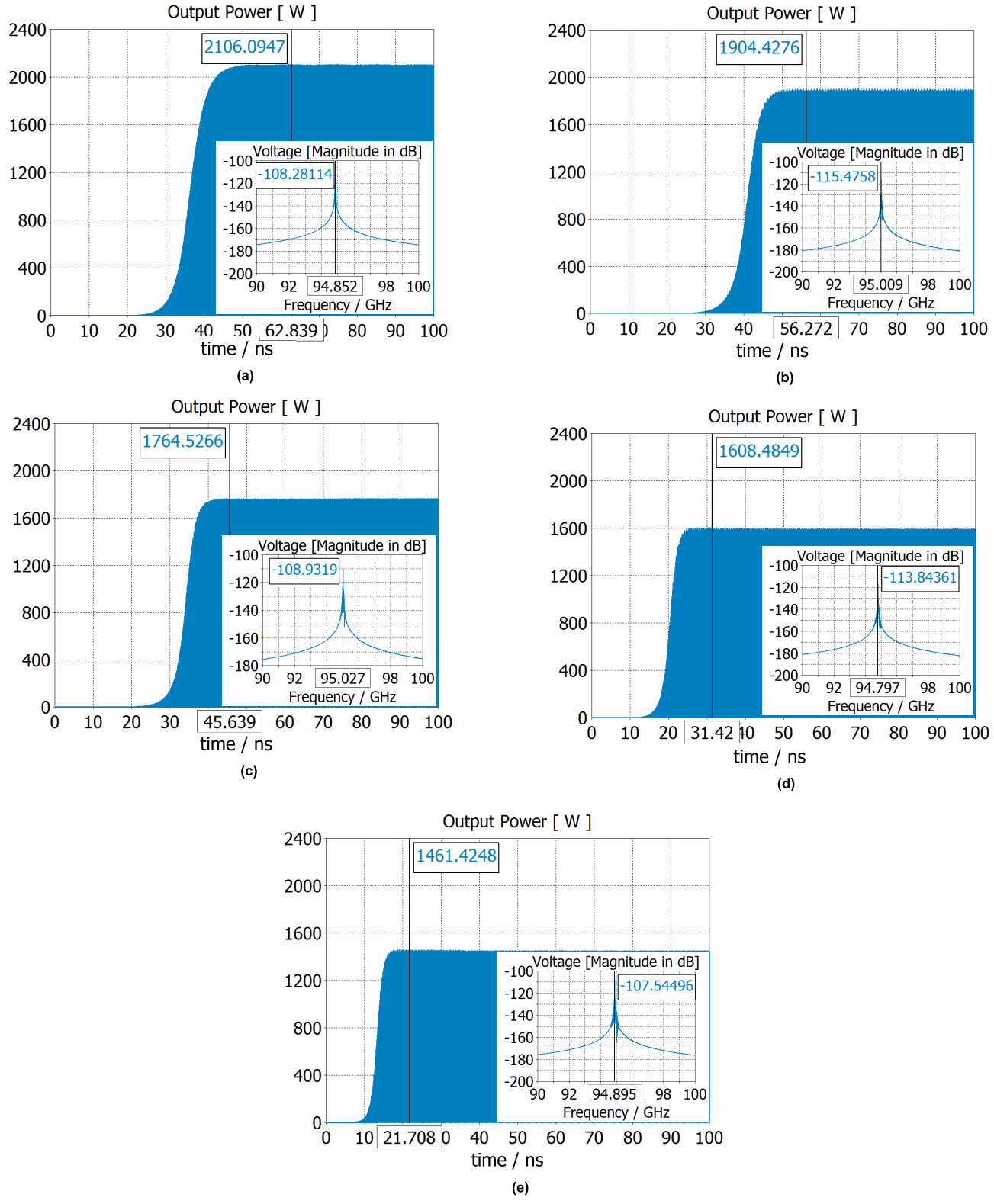

FIGURE 9. The Output power and spectrum of RF signal. (a) N = 5 (b) N = 6 (c) N = 7 (d) N = 8 (e) N = 9.

beam radius, which is conducive to electron bunching, thus leading to improved beam–wave interaction efficiency. The final voltage and current were both at the upper limits set in the program during the optimization process, indicating that the EIO did not reach saturation in this range.

TABLE 4. Comparison of the optimal solutions and PIC models.

	f_0	d(mm)	l(mm)	Q_e	r_b(mm)	R/Q(Ω)	V_0(kV)	I_0(A)	P_{out}(W)	B(MHz)	L_{tot}(mm)
Solution1	95.00	0.45	0.74	975	0.20	181	18.96	0.50	2307	97	3.70
PIC1	94.85	0.45	0.74	1036	0.20	189	19.60	0.50	2106	92	3.70
Δ (%)	0.2	0	0	6.0	0	4.2	3.3	0	9.8	5.4	0
Solution2	95.00	0.46	0.75	589	0.20	218	19.0	0.50	2074	161	4.50
PIC2	95.01	0.46	0.75	638	0.20	231	19.60	0.50	1904	149	4.50
Δ (%)	0	0	0	7.7	0	5.6	3.1	0	8.9	8.1	0
Solution3	95.00	0.48	0.76	441	0.20	245	18.78	0.50	1894	215	5.32
PIC3	95.03	0.48	0.76	474	0.20	262	19.60	0.50	1765	200	5.32
Δ (%)	0	0	0	7.0	0	6.5	4.1	0	7.3	7.5	0
Solution4	95.00	0.49	0.78	314	0.20	290	18.98	0.50	1714	303	6.24
PIC4	94.80	0.49	0.78	327	0.20	315	19.80	0.50	1608	287	6.24
Δ (%)	0.2	0	0	4.0	0	7.9	4.1	0	6.6	5.6	0
Solution5	95.00	0.50	0.79	233	0.20	326	19.00	0.50	1567	408	7.11
PIC5	94.90	0.50	0.79	246	0.20	369	19.90	0.50	1461	386	7.11
Δ (%)	0.1	0	0	5.3	0	11.7	4.5	0	7.3	5.7	0

The above results show that the automatic EIO optimization process yields a set of Pareto optimal solutions that can effectively solve the problem of multiobjective coexistence and express the constraint relationship among different parameters and objectives. Therefore, decision-makers can have more alternative at their disposal choices to fulfill various engineering requirements.

IV. COMPARISON WITH CST-PIC SIMULATION

The proposed optimization procedure is based on the 1D EIO simulation model. However, we need to invert the corresponding 3D model to validate the results. Five typical solution sets (shadowed in TABLE 3) were selected from N = 5 to N = 9, and the corresponding 3D electromagnetic simulation models were established using CST software. Fig. 9 shows the simulation results of these five PIC models. As shown in Fig. 9(a), the 5-gap EIO has a maximum output power of 2106 W and the longest start-up time of more than 60 ns. Moreover, it has a narrow bandwidth and a high quality factor of 1036. Since its characteristic impedance is only 189 Ω, if the quality factor is further reduced, the oscillator will not start up. Figs. 9(b)–(e) show that as the gap number increases, the output power continues to decrease, whereas the start-up time is significantly shortened. The 9-gap EIO benefits from the larger characteristic impedance, which can stabilize the output power at 1461 W in less than 20 ns, and it has a smaller external quality factor of 233 and a wider bandwidth.

A comparison of the specific data obtained using the two methods is given in TABLE 4. The difference in output power can largely be ascribed to the fact that the proposed algorithm is optimized based on a 1D simulation program by ignoring the radial movement of electrons, and the physical model is processed mathematically.

Secondly, the mesh density in the PIC solver and the error in the quality factor evaluated using the time domain solver also affect the output characteristics. However, the results and trends of the PIC simulation are basically consistent with the optimal solutions, and the relative difference is generally within 10%, which is acceptable for the design optimization of high-power devices.

In addition, the automatic design method can significantly increase the EIO optimization efficiency. The simulation of the 3D PIC model required about 10 hours at a time on a computer with an i7-7700 CPU and 16 GB of DDR4 RAM. Thus, with 10 values for each parameter, it will take 10^8 h with 7 input variables to complete all model calculations, and with more input parameters and values, the computation time will increase geometrically. However, when using NSGA-II and the EIO 1D program, the presented optimization algorithm with a population of 50 individuals was run for 500 iterations, and it took less than 100 h to obtain a set of Pareto solutions for multiobjective design. Note that the routing algorithm is the effective solution for processing the relationship among the gap number (length), output power, and bandwidth, which is critical for the optimal design of EIOs.

V. CONCLUSION

This paper describes an automatic optimization solution to optimize multiple objectives of EIOs, such as output power, bandwidth, and structure length. The routing method equates EIO design to a multiobjective optimization problem, completes construction of the decision vector and solution vector, and combines the 1D physical model with the NSGA-II algorithm to obtain a global optimization algorithm. With this approach, a 95-GHz EIO was optimized, and a Pareto set with three optimal objective points was obtained. The distribution characteristics of the structural and electrical parameters in the process of co-transition of multiple goals were described. The final results agreed well with those simulated using the CST-PIC solver, which confirmed that the algorithm was effective for solving the constraints among the multiple design objectives. In addition, instead of the previous single optimal solution, the proposed algorithm yields a set of Pareto solutions, which provides designers with more alternatives.

The optimization procedure presented in this paper has a periodic structure with the equal-amplitude 2 π mode. The equal-amplitude hypothesis is based on the fact that it

cannot only reduce the possibility of breakdown due to high voltage across a certain gap, but also facilitate uniform heat conduction in the slow wave structure. If the phenomena of breakdown, heat dissipation, and miscellaneous mode suppression are effectively solved, this routing algorithm can be applied to more complex real situations, such as the design of aperiodic structures or other operating modes.

REFERENCES

[1] R. J. Barker, N. C. Luhmann, J. H. Booske, and G. S. Nusinovich, *Modern Microwave and Millimeter-Wave Power Electronics*. Hoboken, NJ, USA: Wiley, 2005, pp. 37–43.

[2] A. S. Gilmour, *Klystrons, Traveling Wave Tubes, Magnetrons, Crossed-Field Amplifiers and Gyrotrons*. Norwood, MA, USA: Artech House, 2011, pp. 304–310.

[3] K. Ray Chu, Y.-C. Tsai, T.-T. Yang, M.-H. Tsao, H.-Y. Chen, H. Guo, and L. Chen, "An extended interaction oscillator based on a complex resonator structure," *IEEE Trans. Plasma Sci.*, vol. 28, no. 3, pp. 626–632, Jun. 2000.

[4] A. Roitman, P. Horoyski, B. Steer, and D. Berry, "High power CW 264 GHz tunable extended interaction oscillator," in *Proc. IEEE 14th Int. Vac. Electron. Conf. (IVEC)*, Paris, France, May 2013, pp. 1–2.

[5] P. H. Siegel, "Terahertz technology," *IEEE Trans. Microw. Theory Techn.*, vol. 50, no. 3, pp. 910–928, Mar. 2002.

[6] V. Kesari and B. N. Basu, *High Power Microwave Tubes: Basics and Trends*. San Rafael, CA, USA: Morgan Claypool, 2018, pp. 6.1–6.30.

[7] J. H. Booske, R. J. Dobbs, C. D. Joye, C. L. Kory, G. R. Neil, G.-S. Park, J. Park, and R. J. Temkin, "Vacuum electronic high power terahertz sources," *IEEE Trans. THz Sci. Technol.*, vol. 1, no. 1, pp. 54–75, Sep. 2011.

[8] J. H. Booske, "Plasma physics and related challenges of millimeter-wave-to-terahertz and high power microwave generation," *Phys. Plasmas*, vol. 15, no. 5, May 2008, Art. no. 055502.

[9] R. K. Parker, R. H. Abrams, B. G. Danly, and B. Levush, "Vacuum electronics," *IEEE Trans. Microw. Theory Techn.*, vol. 50, no. 3, pp. 835–845, Mar. 2002.

[10] Z. Chang, L. Meng, Y. Yin, B. Wang, H. Li, A. Rauf, S. Ullah, L. Bi, and R. Peng, "Circuit design of a compact 5-kV W-band extended interaction klystron," *IEEE Trans. Electron Devices*, vol. 65, no. 3, pp. 1179–1184, Mar. 2018.

[11] H. B. Soltani and H. Abiri, "Developing a load-line concept to study the extended interaction oscillators," *IEEE Trans. Electron Devices*, vol. 64, no. 8, pp. 3429–3436, Aug. 2017.

[12] S. Chen, C. Ruan, W. Yong, C. Zhang, D. Zhao, X. Yang, and S. Wang, "Particle-in-cell simulation and optimization of multigap extended output cavity for a W-band sheet-beam EIK," *IEEE Trans. Plasma Sci.*, vol. 42, no. 1, pp. 91–98, Jan. 2014.

[13] R. Xuxun, W. Jianxun, D. Kun, L. Guo, S. Guoxiang, F. Hao, and E. A. Balfour, "Study of a high-efficiency 34-GHz sheet beam extended interaction oscillator with low filling factor," *IEEE Trans. Electron Devices*, vol. 63, no. 10, pp. 4074–4080, Oct. 2016.

[14] H. Tran, G. Lankford, M. E. Read, R. L. Ives, K. Reppert, K. Cline, and J. Guzman, "Optimization of klystron designs using deterministic sampling methods," *IEEE Trans. Electron Devices*, vol. 62, no. 3, pp. 1032–1035, Mar. 2015.

[15] Z. Chen, J. Wang, Y. Wang, H. Qiao, D. Zhang, and W. Guo, "An optimization method of relativistic backward wave oscillator using particle simulation and genetic algorithms," *Phys. Plasmas*, vol. 20, no. 11, Nov. 2013, Art. no. 113103.

[16] C. J. Lingwood, G. Burt, K. J. Gunn, R. G. Carter, R. Marchesin, and E. Jensen, "Automatic optimization of a klystron interaction structure," *IEEE Trans. Electron Devices*, vol. 60, no. 8, pp. 2671–2676, Aug. 2013.

[17] K. Deb, A. Pratap, S. Agarwal, and T. Meyarivan, "A fast and elitist multiobjective genetic algorithm: NSGA-II," *IEEE Trans. Evol. Comput.*, vol. 6, no. 2, pp. 182–197, Apr. 2002.

[18] F. Ren, T. Zhao, J. Jiao, and Y. Hu, "Resilience optimization for complex engineered systems based on the multi-dimensional resilience concept," *IEEE Access*, vol. 5, pp. 19352–19362, 2017.

[19] L. Xiaoqing, D. Haiying, L. Hongwei, L. Mingxue, and S. Zhiqiang, "Optimization control of front-end speed regulation (FESR) wind turbine based on improved NSGA-II," *IEEE Access*, vol. 7, pp. 45583–45593, 2019.

[20] Q. Bian, B. Nener, and X. Wang, "A modified NSGA-II for solving control allocation optimization problem in lateral flight control system for large aircraft," *IEEE Access*, vol. 7, pp. 17696–17704, 2019.

[21] J. Huang, Y. Liu, M. Liu, M. Cao, and Q. Yan, "Multi-objective optimization control of distributed electric drive vehicles based on optimal torque distribution," *IEEE Access*, vol. 7, pp. 16377–16394, 2019.

[22] *CST Microwave Studio*, CST Company, Darmstadt, Germany, 2014.

[23] D. E. Goldberg, *Genetic Algorithms in Search, Optimization and Machine Learning*. Boston, MA, USA: Addison-Wesley, 1989, pp. 197–201.

[24] N. Srinivas and K. Deb, "Multiobjective optimization using nondominated sorting in genetic algorithms," *Evol. Comput.*, vol. 2, no. 3, pp. 221–248, Dec. 1994.

[25] Q. Liu and G. Jiao, "A pipe routing method considering vibration for aero-engine using kriging model and NSGA-II," *IEEE Access*, vol. 6, pp. 6286–6292, 2018.

[26] T. Blickle and L. Thiele, "A comparison of selection schemes used in evolutionary algorithms," *Evol. Comput.*, vol. 4, no. 4, pp. 361–394, Dec. 1996.

[27] B. E. Carlsten and P. J. Tallerico, "Self-consistent klystron simulations," *IEEE Trans. Nucl. Sci.*, vol. 32, no. 5, pp. 2837–2839, Oct. 1985.

[28] H. Yonezawa and Y. Okazaki, "One-dimensional disk model simulation for klystron design," SLAC, Menlo Park, CA, USA, SLAC Tech. Note SLAC-TN-84-5, May 1984.

[29] H. B. Soltani and H. Abiri, "Developing sheet beam klystron simulation capability in AJDISK," *IEEE Trans. Electron Devices*, vol. 64, no. 8, pp. 2430–3429, Aug. 2017.

[30] F. YungSui, Z. Yihsia, and Y. Yiern, "Large signal analysis of an extended interaction oscillator," *Sci. Cinica*, vol. 22, no. 4, pp. 405–416, Apr. 1979.

[31] A. N. Sandalov, V. M. Pikunov, and V. E. Rodyakin, "High efficiency conventional and relativistic klystrons," in *Proc. 3rd Workshop Pulsed RF Sour. Linear Colliders (RF)*, Kanagawa, Japan, Apr. 1996, pp. 175–184.

[32] C. Jian, L. Ji-Run, and Z. M. G. Wei, "Beam-wave synchronization and coupling in a multi-gap coupled cavity," *Acta Phys. Sin.*, vol. 60, no. 5, May 2011, Art. no. 051101.

JIAN CUI was born in Shandong, China, in 1982. He received the Ph.D. degree in physical electronics from the Graduate School, Chinese Academy of Sciences, Beijing, China, in 2011. He is currently with the Information School, North China University of Technology, in the areas of klystrons, generation, and application of microwave and millimeter wave. His research interest includes extended interaction devices.

SHURONG BIAN was born in Benxi, Liaoning, China, in 1996. She received the bachelor's degree in electronic and information engineering from the North China University of Technology, in 2019, where she is currently pursuing the master's degree in information and communication engineering.

AIDI LI was born in Jieshou, Anhui, China, in 1994. She received the master's degree in information and communication engineering from the North China University of Technology, in 2019.